In vitro and *In vivo* Characterization of ^{64}Cu-Labeled Abegrin™, a Humanized Monoclonal Antibody against Integrin $\alpha_v\beta_3$

Weibo Cai,[1] Yun Wu,[1] Kai Chen,[1] Qizhen Cao,[1] David A. Tice,[2] and Xiaoyuan Chen[1]

[1]The Molecular Imaging Program at Stanford, Department of Radiology and Bio-X Program, Stanford University School of Medicine, Stanford, California and [2]MedImmune, Inc., Gaithersburg, Maryland

Abstract

Abegrin™ (MEDI-522 or Vitaxin™), a humanized monoclonal antibody against human integrin $\alpha_v\beta_3$, is in clinical trials for cancer therapy. *In vivo* imaging using Abegrin™-based probes is needed for better treatment monitoring and dose optimization. Here, we conjugated Abegrin™ with macrocyclic chelating agent 1,4,7,10-tetra-azacylododecane *N,N′,N″,N‴*-tetraacetic (DOTA) at five different DOTA/Abegrin™ ratios. The conjugates were labeled with ^{64}Cu (half-life = 12.7 hours) and tested in three human (U87MG, MDA-MB-435, and PC-3) and one mouse (GL-26) tumor models. The *in vitro* and *in vivo* effects of these ^{64}Cu-DOTA-Abegrin™ conjugates were evaluated. The number of DOTA per Abegrin™ varied from 1.65 ± 0.32 to 38.53 ± 5.71 and the radiolabeling yield varied from 5.20 ± 3.16% to 88.12 ± 6.98% (based on 2 mCi ^{64}Cu per 50 μg DOTA-Abegrin™ conjugate). No significant difference in radioimmunoreactivity was found among these conjugates (between 59.78 ± 1.33 % and 71.13 ± 2.58 %). Micro-positron emission tomography studies revealed that ^{64}Cu-DOTA-Abegrin™ (1,000:1) had the highest tumor activity accumulation (49.41 ± 4.54% injected dose/g at 71-hour postinjection for U87MG tumor). The receptor specificity of ^{64}Cu-DOTA-Abegrin was confirmed by effective blocking of MDA-MB-435 tumor uptake with coadministration of nonradioactive Abegrin. ^{64}Cu-DOTA-IgG exhibited background level tumor uptake at all time points examined. Integrin $\alpha_v\beta_3$-specific tumor imaging using ^{64}Cu-DOTA-Abegrin™ may be translated into the clinic to characterize the pharmacokinetics, tumor targeting efficacy, dose optimization, and dose interval of Abegrin™ and/or Abegrin conjugates. Chemotherapeutics or radiotherapeutics using Abegrin™ as the delivering vehicle may also be effective in treating integrin $\alpha_v\beta_3$-positive tumors. (Cancer Res 2006; 66(19): 9673-81)

Introduction

Angiogenesis, the formation of new blood vessels from preexisting vasculature, is a fundamental process occurring during tumor progression and it depends on the balance between proangiogenic molecules and antiangiogenic molecules (1, 2). Cancer cells spread throughout the body by metastasis (3). Interactions between vascular cells and the extracellular matrix (ECM) are involved in multiple steps of tumor angiogenesis and metastasis (4, 5). Integrins, a family of cell adhesion molecules composed of noncovalently associated α and β subunits, are involved in a wide range of cell-ECM and cell-cell interactions (4–6). Inhibition of α_v integrin activity by monoclonal antibodies (mAb), cyclic RGD peptide antagonists, and peptidomimetics has been shown to induce endothelial cell apoptosis, to inhibit angiogenesis, and to increase endothelial monolayer permeability (7, 8). The $\alpha_v\beta_3$ integrin, which recruits and activates matrix metalloproteinase-2 and plasmin to degrade the basement membrane and interstitial matrix (9), is significantly up-regulated on endothelium during angiogenesis but not in quiescent endothelium (4, 5, 7). Integrin $\alpha_v\beta_3$ is also expressed in melanoma, late-stage glioblastoma, ovarian, breast, and prostate cancer cells (10), where it can potentiate metastasis by facilitating cancer cell invasion and movement across blood vessels.

LM609, a mouse anti-human integrin $\alpha_v\beta_3$ mAb, which cross-reacts with $\alpha_v\beta_3$ originated from rabbits, chicken, and hamsters but not from mice and rats, was found to be able to immunoprecipitate integrin $\alpha_v\beta_3$ from M21 human melanoma cells (11). Recognizing the heterodimer as one entity, LM609 is much more specific and superior to other mAbs, which recognizes either the α_v or β_3 subunit. However, being a murine mAb, inefficient interactions with human immune effector cells and the short serum half-life ($t_{1/2}$) of LM609 caused by its immunogenicity in humans severely limits the therapeutic potential of LM609 when chronic administrations are needed (12). For these reasons, LM609 was humanized and later affinity matured as reported previously (13). The humanized version, named Vitaxin™ or Vitaxin I (later named MEDI-523) was used in several phase I clinical trials (13–15). Radioimaging of tumor vasculature using this early version of Vitaxin™ labeled with ^{99m}Tc was unsuccessful due to the instability of the ^{99m}Tc labeling *in vivo* (16). The affinity matured version, now called Abegrin™ (also called Vitaxin™ or MEDI-522), is also in clinical trials. In phase I studies of Abegrin, prolonged stable disease was observed in several patients with renal cell carcinoma and an effect on tumor perfusion was correlated with treatment, although no significant toxicity or immune response was noted at the dose levels tested (17). In 2003, MedImmune, Inc. (Gaithersburg, MD), who licensed Vitaxin™ and designated it as Abegrin™ for clinical development (18), announced the initiation of phase II clinical trials in prostate cancer and melanoma. Recently, the company announced the initiation of phase III for patients with metastatic melanoma based on promising results from their phase II trial with Abegrin™.

We and others have reported small molecule, peptide, protein, and antibody-based probes for fluorescence (19, 20), magnetic resonance (21, 22), ultrasound (23), single-photon emission computed tomography (24, 25), and positron emission tomography (PET; refs. 26–37) imaging of integrin $\alpha_v\beta_3$ expression *in vivo*. To date, most of integrin $\alpha_v\beta_3$ targeted PET studies have been focused on the radio labeling of arginine-glycine-aspartic acid (RGD) peptide antagonists of integrin $\alpha_v\beta_3$ due to their high-binding

Requests for reprints: Xiaoyuan Chen, The Molecular Imaging Program at Stanford, Department of Radiology and Bio-X Program, Stanford University School of Medicine, 1201 Welch Road, P095, Stanford, CA 94305-5484. Phone: 650-725-0950; Fax: 650-736-7925; E-mail: shawchen@stanford.edu.

doi:10.1158/0008-5472.CAN-06-1480

affinity (31, 33, 37, 38). [^{18}F]Galacto-RGD has been tested in healthy volunteers and cancer patients (33, 35). Very recently, we reported that [^{18}F]FRGD2 can be used to quantify tumor integrin $\alpha_v\beta_3$ expression level *in vivo* with static PET scans in xenograft tumor models (29, 37). Both peptide and antibody-based imaging can help in evaluating integrin $\alpha_v\beta_3$ expression level. RGD peptide-based probes are useful in planning and monitoring peptide-based therapeutics due to the similar pharmacokinetics, whereas antibody-based tracer is more relevant to antibody-based therapy. The relatively longer $t_{1/2}$ of ^{64}Cu [$t_{1/2}$ = 12.7 hours; β^+ = 655 keV (17%); β^- = 573 keV (39%)] is well suited for the mAb labeling and imaging. To date, no imaging using Abegrin™ has been reported. Here, we report the first ^{64}Cu-labeled Abegrin™ through 1,4,7,10-tetra-azacylododecane *N,N′,N″,N‴*-tetraacetic (DOTA) chelator and the *in vitro* as well as *in vivo* characterizations of the resulting ^{64}Cu-DOTA-Abegrin™.

Materials and Methods

All commercially available chemical reagents were used without further purification. DOTA was purchased from Macrocyclics, Inc. (Dallas, TX). 1-Ethyl-3-[3-(dimethylamino)-propyl] carbodiimide (EDC), *N*-hydroxysulfonosuccinimide (SNHS), and Chelex 100 resin (50-100 mesh) were purchased from Sigma-Aldrich (St. Louis, MO). Water and all buffers were passed through Chelex 100 column before use in radiolabeling procedures to ensure that the aqueous buffer is heavy metal-free. The syringe filter, polyethersulfone membranes (pore size, 0.2 μm; diameter, 13 mm) were obtained from Nalge Nunc International (Rochester, NY). ^{125}I-Echistatin and PD-10 desalting column were purchased from GE Healthcare (Piscataway, NJ). Female athymic nude mice were supplied from Harlan (Indianapolis, IN) at 4 to 5 weeks of age. ^{64}Cu was obtained from Washington University (St. Louis, MO) and University of Wisconsin (Madison, WI). ^{64}Cu was produced using the ^{64}Ni(p,n)^{64}Cu nuclear reaction and supplied in high specific activity as $^{64}CuCl_2$ in 0.1 mol/L HCl.

DOTA conjugation and radiolabeling. DOTA was activated by EDC and SNHS at pH 5.5 for 30 minutes with a molar ratio of 10:5:4 (DOTA/EDC/SNHS). Without purification, the DOTA-*N*-hydroxysulfosuccinimidyl (OSSu) was cooled to 4°C and added to Abegrin at five different molar ratios (DOTA-OSSu/Abegrin™ of 20:1, 50:1, 100:1, 200:1, and 1,000:1). The reaction mixture was adjusted to pH 8.5 with 0.1 N of NaOH and allowed to incubate for overnight at 4°C. The DOTA-Abegrin conjugates were then purified by PD-10 column and concentrated by Centricon filter (Millipore, Bedford, MA), and the final concentration was measured based on UV absorbance at 280 nm using unconjugated Abegrin™ of known concentrations as standard. $^{64}CuCl_2$ (2 mCi) was diluted in 300 μL of 0.1 mol/L sodium acetate buffer (pH 6.5) and added to the DOTA-Abegrin™ conjugates (25 μg DOTA-Abegrin™/mCi of ^{64}Cu). The reaction mixture was incubated for 1 hour at 40°C with constant shaking. The ^{64}Cu-DOTA-Abegrin™ conjugates were then purified by PD-10 column using PBS as the mobile phase. The radioactive fractions containing ^{64}Cu-DOTA-Abegrin™ was collected and passed through a 0.2-μm syringe filter for further *in vitro* and *in vivo* experiments.

Number of DOTA per Abegrin™ and immunoreactivity. The average number of DOTA chelators per Abegrin™ antibody was determined using a previously reported procedure with slight modifications (39). Briefly, a defined amount of nonradioactive $CuCl_2$ (80-fold excess of DOTA-Abegrin™) in 40 μL 0.1 N sodium acetate (NaOAc) buffer (pH 6.5) was added to 1.0 mCi $^{64}CuCl_2$ in 20 μL 0.1 N NaOAc buffer, and 20 μg of each DOTA-Abegrin™ conjugate in 90 μL 0.1 N NaOAc buffer were added to the above carrier-added $^{64}CuCl_2$ solution. The reaction mixture was incubated with constant shaking at 40°C for 1 hour. The ^{64}Cu-DOTA-Abegrin™ was purified using PD-10 column and the radiolabeling yield was calculated. The number of DOTA per Abegrin™ was calculated using the following equation: number of DOTA per Abegrin™ = moles (Cu^{2+}) × yield/moles (DOTA-Abegrin™). The results were expressed as mean ± SD (n = 3). An isotype control IgG (against a bacterial antigen with no cross-reaction with human or mouse integrin $\alpha_v\beta_3$; supplied by MedImmune) was conjugated with DOTA under the same condition and the number of DOTA per IgG was also determined as described above.

The immunoreactivity of each ^{64}Cu-DOTA-Abegrin™ conjugate (with different number of DOTA per Abegrin™) was determined by incubating with integrin $\alpha_v\beta_3$-positive U87MG cells in suspension culture under conditions of antigen excess (n = 3; ref. 40). The immunoreactivity was calculated as follows: immunoreactivity = bound activity on cells/total added activity × 100%.

Cell lines and cell integrin receptor assay. Four cell lines were used for *in vitro* and *in vivo* experiments. U87MG human glioblastoma, MDA-MB-435 human breast cancer carcinoma, and PC-3 human prostate adenocarcinoma cell lines were obtained from American Type Culture Collection (Manassas, VA). The GL-26 mouse glioblastoma cell line was kindly provided by Dr. Victor K. Tse (Department of Neurosurgery, Stanford University, Stanford, CA). All culture media were obtained from Invitrogen Corp. (Carlsbad, CA). U87MG cells were grown in DMEM (low glucose), MDA-MB-435 cells were grown in Leibovitz's L-15 Medium, PC-3 cells were grown in F-12K nutrient mixture (Kaighn's Modification), and GL-26 cells were grown in DMEM (high glucose). All cell lines were cultured in medium supplemented with 10% (v/v) fetal bovine serum at 37°C in a humidified atmosphere with 5% CO_2, except for MDA-MB-435, which was cultured without CO_2. The procedure of cell integrin receptor assay has been reported earlier (29, 41).

Flow cytometry. Cells were collected and washed with PBS and incubated with Abegrin™ (20 μg/mL) in PBS supplemented with 1% bovine serum albumin (BSA) for 30 minutes at 4°C. After washing with PBS containing 1% BSA, the cells were incubated with FITC donkey anti-human IgG (1:100; Jackson ImmunoResearch Laboratories, Inc., West Grove, CA) for 30 minutes at 4°C. The cells were washed again, resuspended in PBS, and analyzed using a LSR model 1A analyzer (Becton Dickinson, Heidelberg, Germany) and FlowJo analysis software (Tree Star, Inc., Ashland, OR).

Animal models. Animal procedures were done according to a protocol approved by Stanford University Institutional Animal Care and Use Committee. The MDA-MB-435 breast cancer model was established by orthotopic injection of 5×10^6 cells (in 50 μL PBS) into the left mammary fat pad. The U87MG, PC-3, and GL-26 tumor models were obtained by s.c. injection of the corresponding cells (5×10^6 in 50 μL PBS) into the right front leg of the mice (male mice were used for PC-3 tumor). The mice were subjected to microPET imaging and biodistribution studies when the tumor volume reached 200 to 500 mm^3 (2 weeks after inoculation for GL-26 tumor model; 3-4 weeks after inoculation for U87MG, MDA-MB-435, and PC-3 tumor models).

MicroPET imaging studies. PET imaging of tumor-bearing mice was done on a microPET R4 rodent model scanner (Concorde Microsystems, Knoxville, TN). The scanner has computer controlled vertical and horizontal bed motion, with an effective axial field of view (FOV) of 7.8 cm and transaxial FOV of 10 cm. The tumor-bearing mice were imaged in prone position in the microPET scanner. The mice were injected with 200 to 300 μCi ^{64}Cu-DOTA-Abegrin™ via the tail vein, anesthetized with 2% isoflurane, and placed near the center of the FOV where the highest image resolution and sensitivity is available. Three- to five-minute static scans were done before 24-hour postinjection, whereas 10- to 20-minute static scans were carried out after 24-hour postinjection For each microPET scan, three-dimensional regions of interests (ROI) were drawn over the tumor, heart, liver, kidneys, and muscle on decay-corrected whole-body coronal images. The average radioactivity concentration (accumulation) within a tumor or an organ was obtained from mean pixel values within the ROI volume, which were converted to counts per milliliter per minute by using a conversion factor. Assuming a tissue density of 1 g/mL, the counts per milliliter per minute were converted to counts per gram per minute and then divided by the injected dose (ID) to obtain an imaging ROI-derived percent injected dose per gram of tissue (% ID/g) of tissue. A mouse bearing a MDA-MB-435 tumor was also imaged using ^{64}Cu-DOTA-Abegrin™ coinjected with 2 mg of unconjugated Abegrin. As a control experiment, ^{64}Cu-DOTA-IgG (200-300 μCi) was injected into U87MG tumor-bearing mice and microPET scans were done as described above.

Table 1. The radiolabeling yield, number of DOTA per Abegrin™, specific activity, and immunoreactivity of the five ^{64}Cu-DOTA-Abegrin™ conjugates

DOTA/Abegrin ratio	20:1	50:1	100:1	200:1	1,000:1
Yield (%)	5.20 ± 3.16	14.05 ± 17.12	25.32 ± 11.50	37.32 ± 25.94	88.12 ± 6.98
No. of DOTA per Abegrin™	1.65 ± 0.32	3.29 ± 2.01	6.38 ± 3.52	9.66 ± 3.39	38.53 ± 5.71
No. specific activity (mCi/mg)	2.11 ± 1.28	6.65 ± 8.10	11.14 ± 5.06	15.23 ± 10.59	25.89 ± 2.05
Immunoreactivity (%)	59.78 ± 1.33	61.01 ± 6.88	71.13 ± 2.58	65.61 ± 6.14	62.74 ± 8.29

Biodistribution studies. Female nude mice bearing MDA-MB-435 tumors were injected with about 20 μCi ^{64}Cu-DOTA-Abegrin™. The mice were sacrificed and dissected at 18-, 44-, and 68-hour postinjection. Blood, tumor, major organs, and tissues were collected and wet weighed. The radioactivity in the tissues was measured using a gamma counter (Packard, Meriden, CT). The results were presented as %ID/g. For each mouse, the radioactivity of the tissue samples was calibrated against a known aliquot of the injectate and normalized to a body weight of 20 g. Values are presented as mean ± SD for a group of three animals.

Radiation dosimetry extrapolation to human. Estimated human dosimetry was calculated from microPET imaging results on Sprague-Dawley female rats (Harlan) injected with ^{64}Cu-DOTA-Abegrin™. The rats were scanned at two bed positions to cover the whole body and ROI analysis were carried out on major organs. Time-activity curves were generated from the mean values obtained in rats for each organ of interest. We then calculated source organ residence times for the human model by integrating a monoexponential fit to the experimental biodistribution data for major organs (heart, lung, liver, kidneys, and spleen) and the whole body. The source organ residence times obtained forthwith were used with a standard quantitation platform organ level internal dose assessment (Vanderbilt University, Nashville TN; ref. 42).

Immunofluorescence staining. Frozen tumor sections were warmed to room temperature, fixed with ice-cold acetone for 10 minutes, and dried in the air for 30 minutes. The sections were blocked with 10% donkey serum for 1 hour at room temperature. For CD31 and human integrin $\alpha_v\beta_3$ double staining, the sections were incubated with rat anti-mouse CD31 (1:100; BD Biosciences, San Jose, CA) and Abegrin™ (100 μg/mL) for 1 hour at room temperature. After incubating with Cy3-conjugated donkey anti-mouse secondary antibody (1:200; Jackson ImmunoResearch Laboratories) and FITC-conjugated donkey anti-human secondary antibody (1:200), the tumor sections were examined under the microscope (Carl Zeiss Axiovert 200M, Carl Zeiss, Thornwood, NY). For CD31 and mouse integrin β_3 double staining, hamster anti-mouse β_3 (1:100) and FITC-conjugated goat anti-hamster secondary antibody (1:400; Jackson ImmunoResearch Laboratories) were used.

Statistical analysis. Quantitative data were expressed as mean ± SD. Means were compared using one-way ANOVA and Student's *t* test. *P*s < 0.05 were considered statistically significant.

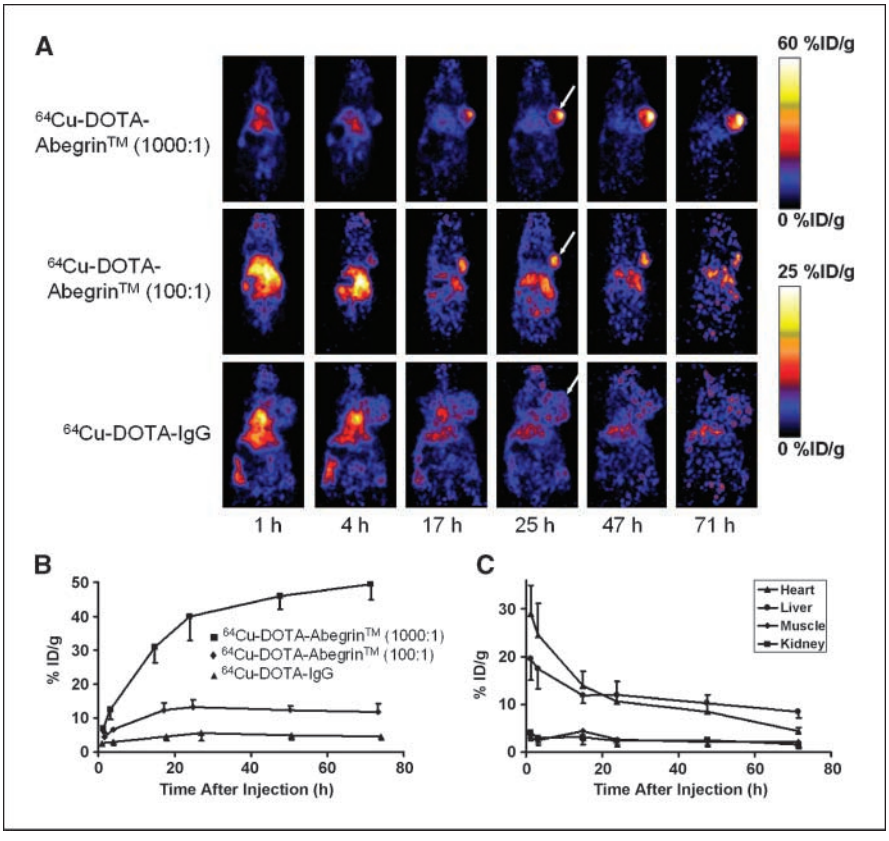

Figure 1. *A,* serial microPET scans of U87MG tumor-bearing mice after injection of ^{64}Cu-DOTA-Abegrin™ (1,000:1), ^{64}Cu-DOTA-Abegrin (100:1), and ^{64}Cu-DOTA-IgG (three mice per group). Note that the scale for ^{64}Cu-DOTA-Abegrin™ (1,000:1) is 0 to 60 %ID/g, whereas the scale for the other two conjugates is 0 to 25 %ID/g. Decay-corrected whole-body coronal images that contain the tumor. *B,* time activity curves of U87MG tumor uptake for the three tracers described above (three mice per group). *C,* time activity curves of the heart, liver, kidney, and muscle of ^{64}Cu-DOTA-Abegrin™ (1,000:1; 3 mice per group). Tracer uptake of other organs is at similar level as the muscle and the kidney.

Results

Number of DOTA per Abegrin™, radiolabeling yield, specific activity, and immunoreactivity. Five different reaction ratios were tested for DOTA-Abegrin™ conjugation (Table 1). For the DOTA/Abegrin™ ratio of 20:1, 50:1, 100:1, 200:1, and 1,000:1 used for conjugation reaction, the number of DOTA per Abegrin™ was determined to be between 1.65 ± 0.32 and 38.53 ± 5.71. The reaction conditions and the amount of ^{64}Cu and each DOTA-Abegrin™ conjugate used for the radiolabeling were quite similar. Because the radiolabeling yield varied from 5.20 ± 3.16% to 88.12 ± 6.98%, the specific activity of the resulting ^{64}Cu-DOTA-Abegrin™ also varied from 2.11 ± 1.28 to 25.89 ± 2.05 mCi/mg Abegrin™. Although the number of DOTA per Abegrin™ was quite different for the five conjugates, the immunoreactivity was similar and all of them were about 60% to 70%, suggesting that the accessible lysine residues were largely away from the complementarity-determining region. ^{64}Cu-DOTA-IgG was determined to have 24.08 ± 0.42 DOTA residues per IgG (n = 3) and the ^{64}Cu-labeling yield was about 85 % under similar conditions.

MicroPET studies of ^{64}Cu-DOTA-Abegrin™ conjugates in U87MG tumor-bearing mice. As can be seen in Fig. 1*A*, the tumor uptake of ^{64}Cu-DOTA-Abegrin™ (1,000:1) was significantly higher than ^{64}Cu-DOTA-Abegrin™ (100:1; P < 0.05 at all time points examined). All five conjugates with different DOTA/Abegrin ratio exhibited good tumor contrast (data not shown for the other three conjugates). Note that the scale for ^{64}Cu-DOTA-Abegrin™ (1,000:1) was 0 to 60 %ID/g and the scale for ^{64}Cu-DOTA-Abegrin™ (100:1) was 0 to 25 %ID/g. MicroPET imaging of the same tumor model with ^{64}Cu-DOTA-IgG did not give significant tumor uptake above the background (P < 0.05 at all time points when compared with ^{64}Cu-DOTA-Abegrin™; 1,000:1). The U87MG tumor uptake of ^{64}Cu-DOTA-Abegrin™ (1,000:1) increased with time and reached a plateau at about 24-hour postinjection. The tumor uptake was 12.50 ± 2.73, 39.88 ± 7.05, and 49.41 ± 4.54 %ID/g at 4-, 25-, and 71-hour postinjection, respectively (Fig. 1*B*). All five conjugates exhibited high uptake in the heart (due to blood pool activity) and liver (due to the nonspecific uptake of the tracer by the reticuloendothelial system) at early time points, whereas the tracer uptake in all the other organs was at the background level. No significant difference was observed between the five conjugates in either the uptake level of the tracer in the major organs or the washout pattern. As can be seen in Fig. 1*C*, the tracer uptake in both the heart and the liver dropped steadily over time. For the heart, the uptake was 29.08 ± 5.90, 13.89 ± 3.13, 8.45 ± 3.59, and 4.38 ± 0.82 %ID/g at 1-, 17-, 47-, and 71-hour postinjection, respectively, indicating that the serum $t_{1/2}$ of the tracer was about 12 to 24 hours in the mouse. For the liver, the uptake was 19.56 ± 4.43, 11.91 ± 1.68, 10.24 ± 2.05, and 8.51 ± 1.31 %ID/g at 1-, 17-, 47-, and 71-hour postinjection, respectively. The small fraction of ^{64}Cu dissociated from the DOTA chelator did not cause appreciable increase of liver uptake over the time course of this study. Based on the immunoreactivity and microPET imaging results, ^{64}Cu-DOTA-Abegrin™ (1,000:1) was used for all the following studies and it will be referred to as ^{64}Cu-DOTA-Abegrin™ in the following text.

Fluorescence-activated cell sorting analysis and cell integrin $\alpha_v\beta_3$ expression level. Fluorescence-activated cell sorting (FACS) analysis using Abegrin as the primary antibody against integrin $\alpha_v\beta_3$ clearly showed that U87MG, PC-3, and MDA-MB-435 cells are integrin $\alpha_v\beta_3$ positive (Fig. 2*A*). Although GL-26 cells are mouse integrin $\alpha_v\beta_3$ positive (where anti-mouse β_3 mAb was used as the primary antibody; Fig. 2*A, bottom, right*), it is not recognized by Abegrin, which showed that Abegrin™ is human integrin $\alpha_v\beta_3$ specific and does not cross-react with mouse $\alpha_v\beta_3$. Next, we quantified the $\alpha_v\beta_3$ integrin expression level of the four cell lines through competitive cell-binding assay using ^{125}I-echistatin as radioligand. The density of integrin $\alpha_v\beta_3$ on the cell surface follows the order U87MG > MDA-MB-435 > GL-26 ≈ PC-3 (Fig. 2*B*). Note that echistatin binds to integrin $\alpha_v\beta_3$ as one entity but not integrin α_v or integrin β_3 alone and it recognizes both human and mouse integrin $\alpha_v\beta_3$.

MicroPET imaging of tumor models with different integrin $\alpha_v\beta_3$ expression level. The localization of ^{64}Cu-DOTA-Abegrin™ in all four tumor models was evaluated by multiple time point microPET imaging. Selected coronal images at different time points postinjection were shown in Fig. 3*A*. At 4-hour postinjection, the tumor was already visible. The tumor signal at this early time point may be due to both specific targeting and nonspecific targeting because of the enhanced permeability and retention (EPR) effect, as tumors have abnormal and leaky vasculature and lack lymphatic drainage. High tumor activity accumulation was observed as early as 17-hour postinjection The tumor signal of U87MG-, PC-3-, and MDA-MB-435-bearing mice increased over time (Fig. 3*B*), indicating specific binding between Abegrin and human integrin $\alpha_v\beta_3$. The tumor signal intensity was similar for MDA-MB-435 and PC-3 tumors, whereas the U87MG tumor uptake is much higher

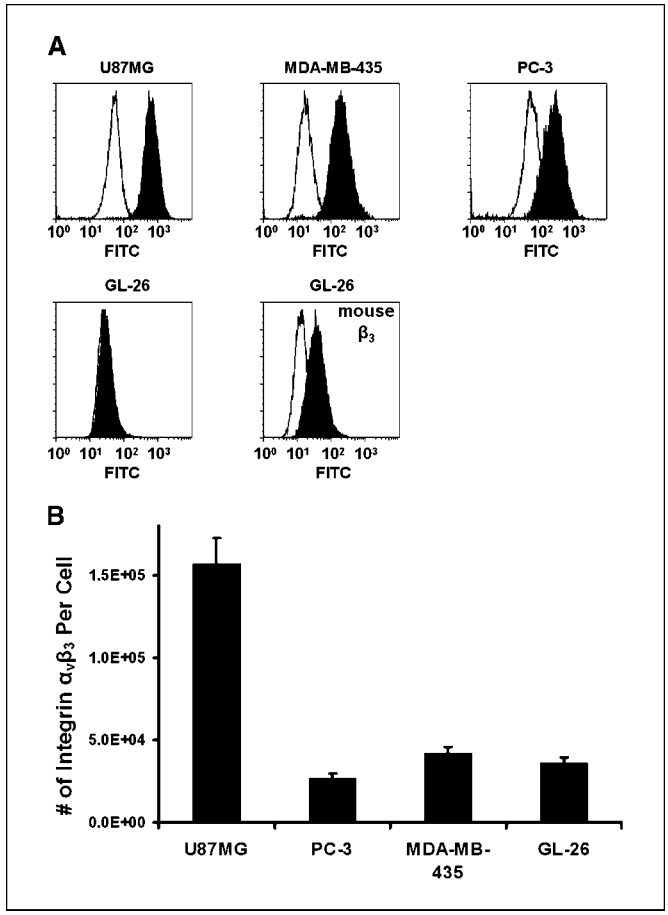

Figure 2. *A,* FACS analysis of four tumor cell lines (U87MG, MDA-MB-435, PC-3, and GL-26) using Abegrin as the primary antibody. *Bottom, right,* anti-mouse β_3 antibody was used. *B,* the number of integrin $\alpha_v\beta_3$ per cell for the four cell lines.

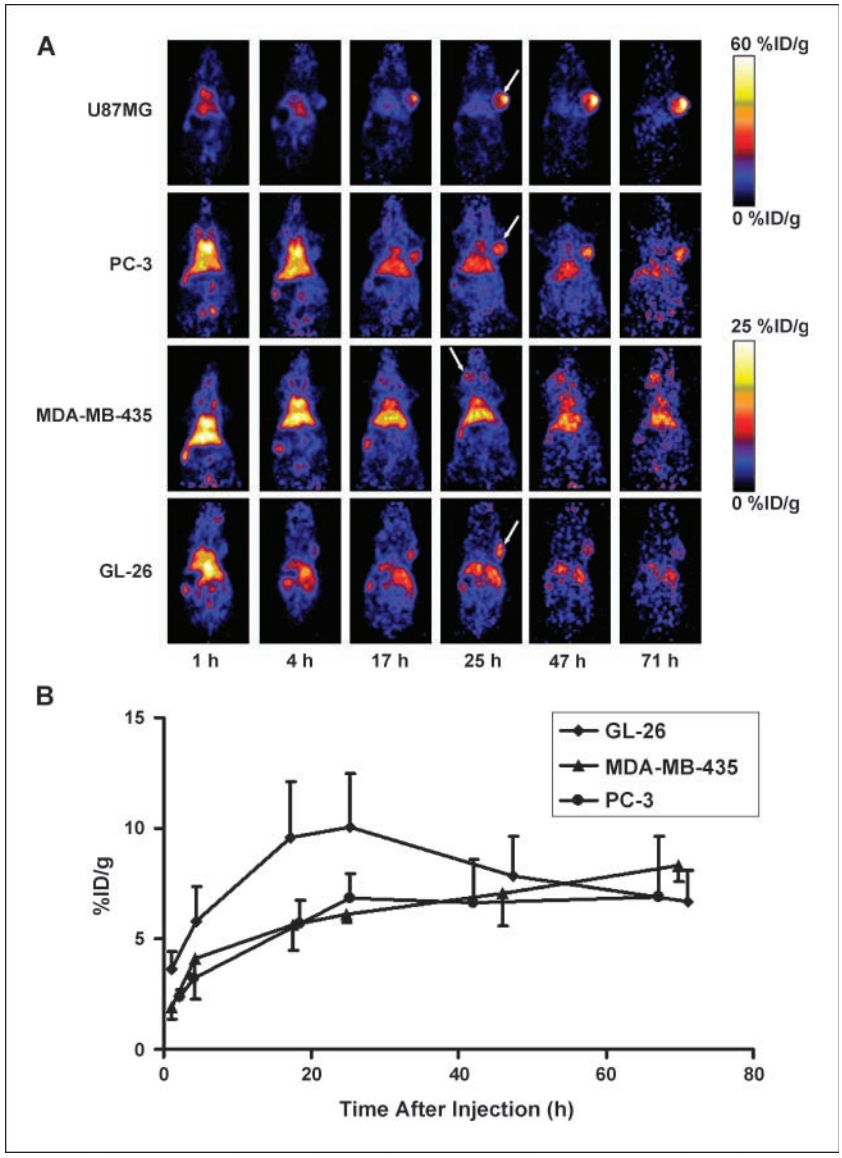

Figure 3. *A,* serial microPET scans of mice bearing different tumors after injection of ^{64}Cu-DOTA-Abegrin^{TM} (three mice per group). Note that the scale for U87MG is 0 to 60 %ID/g, whereas the scale for the other three groups is 0 to 25 %ID/g. *B,* time activity curves of ^{64}Cu-DOTA-Abegrin^{TM} uptake in GL-26, PC-3, and MDA-MB-435 tumors (three mice per group). Note the difference in tracer uptake profile of GL-26 compared with the other two tumor models.

(Fig. 1*B*), agreeing with the cell integrin receptor level. The fact that the GL-26 tumor signal intensity reached a peak at 24-hour postinjection and steadily dropped afterwards is indicative of passive targeting due to the EPR effect, corroborating with the FACS analysis data because Abegrin does not cross-react with mouse integrin $\alpha_v\beta_3$. As all tumor models in this study are murine xenografts, the integrin $\alpha_v\beta_3$ expressed on the tumor vasculature is of mouse origin and is not recognized by Abegrin^{TM}. The uptake profile in the heart, liver, kidneys, and muscle were similar in all four tumor models.

Immunofluorescence staining. After the microPET studies and the radioactivity mostly decayed, the mice were sacrificed and frozen tumor sections were stained for CD31, human integrin $\alpha_v\beta_3$, and mouse integrin β_3. Only the images of U87MG and GL-26 tumors were shown. As can be seen from Fig. 4*A*, the CD31 and mouse β_3 staining colocalizes very well, indicating that the tumor vasculature expresses mouse integrin $\alpha_v\beta_3$. For the GL-26 tumor, both the tumor vasculature and the GL-26 tumor cell express mouse integrin $\alpha_v\beta_3$ as evidenced by the staining (anti-mouse β_3 antibody stains both the tumor cells and the tumor vasculature). When using Abegrin as the primary antibody, there is no colocalization with CD31 for the U87MG tumor because only the human tumor cells but not the mouse tumor vasculature are recognized by Abegrin^{TM} (Fig. 4*B*). For GL-26 tumor, no Abegrin staining was visible as neither the tumor vasculature nor the tumor cells express human integrin $\alpha_v\beta_3$. *Ex vivo* staining experiments again confirmed the human integrin $\alpha_v\beta_3$-specific binding of Abegrin.

Blocking experiment and biodistribution studies. Blocking studies were carried out in a MDA-MB-435 tumor-bearing mouse by coinjecting ^{64}Cu-DOTA-Abegrin^{TM} with 2 mg Abegrin^{TM}. Serial microPET imaging clearly showed much lower tumor uptake of the tracer under blocking conditions (Fig. 5*A*). Effective blocking showed the integrin $\alpha_v\beta_3$-specific binding of ^{64}Cu-DOTA-Abegrin^{TM}. Biodistribution of ^{64}Cu-DOTA-Abegrin^{TM} was also carried out in the MDA-MB-435 tumor model at 18-, 44-, and 68-hour postinjection (Fig. 5*B*). It can be seen that the major tracer clearance is through the liver and the spleen. All other organs had

background level uptake of the tracer, providing good tumor contrast of the tracer. The MDA-MB-435 tumor uptake was 4.54 ± 0.39 %ID/g based on biodistribution studies and 5.63 ± 1.16 %ID/g based on microPET studies at 18-hour postinjection (P = 0.17). At 46-hour postinjection, the MDA-MB-435 tumor uptake was 5.40 ± 0.75 %ID/g based on biodistribution experiments and 7.04 ± 1.47 %ID/g based on microPET studies, respectively (P = 0.16). Comparing the quantification results of the tracer uptake between microPET and biodistribution studies, the uptake in all the other organs follow similar pattern, indicating that the quantification methods used for the noninvasive microPET study is a true reflection of the tracer uptake *in vivo*.

Radiation dosimetry. Human absorbed doses to normal organs from ^{64}Cu-DOTA-Abegrin™ were estimated from microPET imaging data in Sprague-Dawley rats and presented in Table 2. The tracer uptake of different organs in rats is similar to that of the mice, except that the liver uptake in the rats appears to be more prominent and persistent (Fig. 5*C*). Except for the heart, liver, and spleen, all other organs exhibited background level of tracer uptake at all time points examined. There is no significant kidney uptake or renal excretion of the mAb-based tracer due to the high molecular weight (150 kDa). These results predict that the highest radiation-absorbed doses will be to the liver (0.33 ± 0.02 mGy/MBq) and spleen (0.21 ± 0.01 mGy/MBq). The whole-body absorbed dose was found to be 0.034 ± 0.001 mGy/MBq. Although the radiation doses to liver and spleen are higher than other ^{64}Cu-labeled mAb reported in the literature (43), the doses to other major organs (kidneys, lungs, intestines, etc.) are much lower.

Discussion

This study shows that ^{64}Cu-labeled Abegrin™, a humanized mAb against human integrin $\alpha_v\beta_3$, exhibits high integrin $\alpha_v\beta_3$ specificity *in vitro* and *in vivo*. As Abegrin™ is currently in phase I/II clinical trials and soon to enter phase III, PET imaging is critical in early and sensitive lesion detection, patient selection for clinical trials based on *in vivo* integrin expression quantification, better treatment monitoring and dose optimization, and elucidation of the mechanisms of treatment efficacy underlying integrin signaling.

We have optimized the DOTA/Abegrin™ ratio for better *in vivo* targeting and maximized tumor uptake. As the equivalence of DOTA used for conjugation reaction increases, the number of DOTA residues per Abegrin™, the specific activity of the tracer, as well as the absolute tracer uptake in the tumor all increases. Because the difference in immumoreactivity is minimal between the five tracers, the conjugate with the most DOTA residues per Abegrin™ is more suitable for future clinical translation. The fact that DOTA conjugation of Abegrin™ does not deteriorate the receptor affinity of the antibody indicates that the accessible lysine residues are mostly located away from the antigen-binding site. High specific activity may also play a role here. It has been reported previously that a dendrimer-mAb conjugate with high specific activity exhibited higher tumor uptake (44). Although not tested, we envision that Abegrin coupled to dendrimeric DOTAs may give comparable or potentially even higher tumor uptake. Due to the relatively high molecular weight of the mAb (150 kDa), the tracer exhibited mainly hepatic clearance. Intact IgG is designed to remain in the bloodstream for many weeks, which is of considerable advantage when acting in the natural setting of

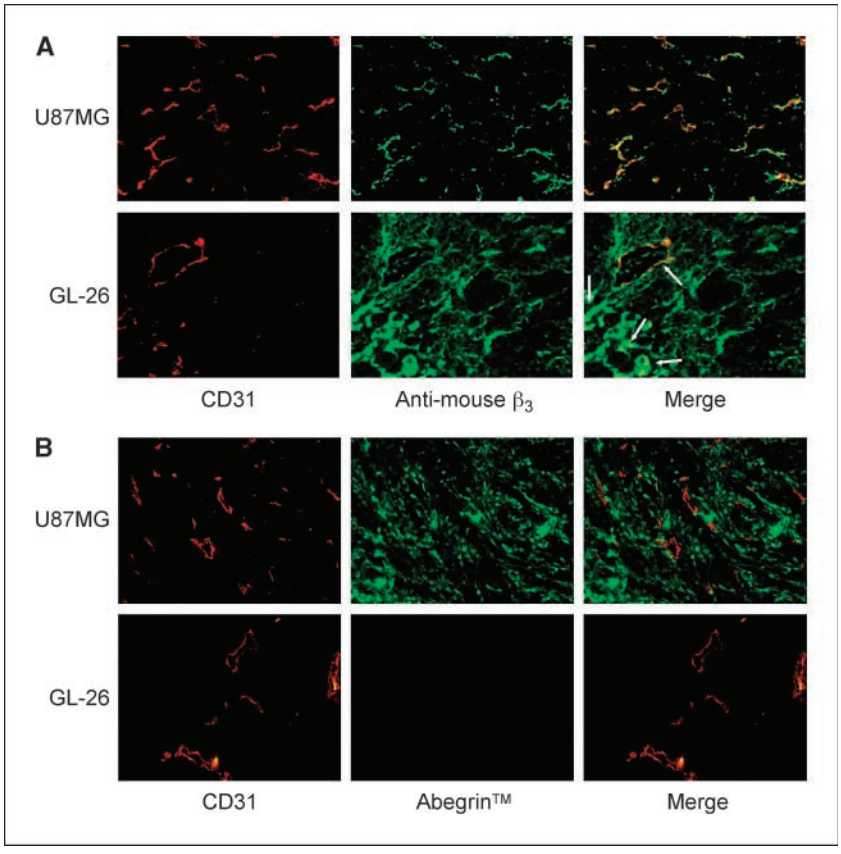

Figure 4. *A*, CD31 and mouse β_3 staining of U87MG and GL-26 tumor sections. *Arrows*, colocalizations for the GL-26 tumor. *B*, CD31 and Abegrin™ staining of U87MG and GL-26 tumors.

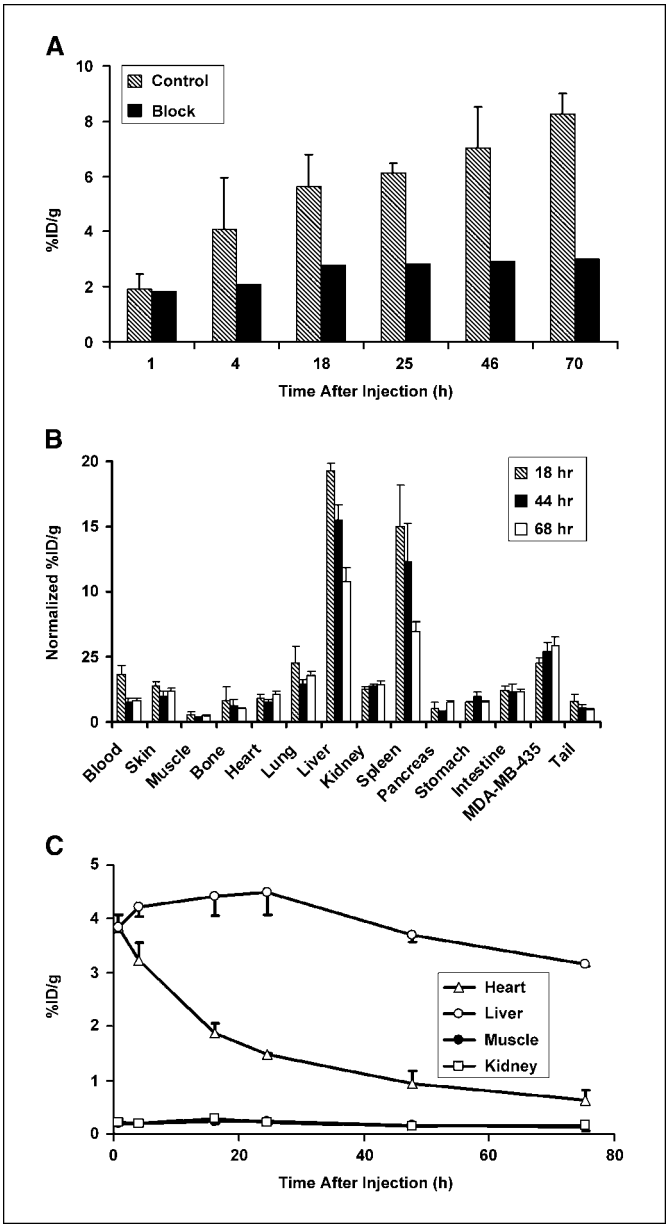

Figure 5. *A,* MDA-MB-435 tumor uptake of ^{64}Cu-DOTA-Abegrin^{TM} injected with (block) and without (control) 2 mg of unlabeled Abegrin^{TM}. *B,* biodistribution at different time points postinjection for ^{64}Cu-DOTA-Abegrin^{TM} in female athymic nude mice bearing orthotopic MDA-MB-435 tumors (three mice per group). *C,* time activity curves of major organ uptake of ^{64}Cu-DOTA-Abegrin^{TM} in female rats (n = 3).

removing foreign entities. The serum $t_{1/2}$ of ^{64}Cu-DOTA-Abegrin^{TM} in mouse is about 12 to 24 hours based on microPET studies, much shorter than the $t_{1/2}$ in humans (5-8 days; ref. 17), presumably due to the much faster metabolic rate of mouse compared with human. In this study, we followed the tracer uptake for about 72 hours (almost six $t_{1/2}$ of ^{64}Cu). Longer term monitoring may be necessary for future studies and ^{89}Zr with a $t_{1/2}$ of 79.3 hours can be used. It has been reported that ^{89}Zr imaging might be a good reflection of ^{90}Y distribution (45), which may shed light on future radioimmunotherapy studies using ^{90}Y-Abegrin^{TM} conjugates.

For antiangiogenic treatment using Abegrin alone or in combination with other treatment modalities, the long circulation $t_{1/2}$ is advantageous because less administration is needed to maintain serum levels of the antibody. The very high tracer uptake in the tumor (up to 49.41 $\pm$ 4.54 %ID/g in the U87MG tumor) along with minimal signal in the nontargeting organs warrants future radioimmunotherapy studies using DOTA-Abegrin^{TM}, as therapeutic radioisotopes (^{67}Cu, ^{177}Lu, ^{90}Y, etc.) can be incorporated using a similar strategy. Previous report has shown prominent expression of integrin $\alpha_v\beta_3$ by glioma cells and vasculature in cancer patients, especially in the periphery of high-grade gliomas (46). Systematic investigation of $\alpha_v\beta_3$ expression on tumor-associated vessels in cancer patients also revealed that a considerable number of colon, pancreas, lung, and breast carcinoma lesions have many $\alpha_v\beta_3$-expressing vessels that could be targets for anti-integrin $\alpha_v\beta_3$ therapy (47). Clinical translation of ^{64}Cu-DOTA-Abegrin^{TM} will be critical for the maximum benefit of Abegrin-based anticancer agents as imaging can provide a straightforward and convenient way to monitor the biological changes at the molecular level *in vivo*.

Abegrin is a humanized antibody, which recognizes only human but not murine integrin $\alpha_v\beta_3$. Both the microPET imaging studies and the immunofluorescence staining confirmed that Abegrin^{TM} does not bind to mouse tumor vasculature. Therefore, the difference in tumor uptake is a good reflection of the integrin $\alpha_v\beta_3$ expression level of different tumor cells. For GL-26 tumor, which only expresses murine integrin $\alpha_v\beta_3$, the tracer uptake is mostly nonspecific. As can be seen from Fig. 3*B*, the tracer uptake in the tumor reached maximum at about 24-hour postinjection and dropped steadily afterwards. This is characteristic of passive

Table 2. Estimated radiation absorbed doses to an adult human after i.v. injection of ^{64}Cu-DOTA-Abegrin^{TM} based on the microPET imaging data obtained in Sprague-Dawley rats (n = 3)

Organ	mGy/MBq (SD)	rad/mCi (SD)
Adrenals	3.16E-02 (2.00E-04)	1.17E-01 (1.00E-03)
Brain	1.47E-02 (6.03E-04)	5.45E-02 (2.23E-03)
Breasts	1.71E-02 (4.04E-04)	6.33E-02 (1.51E-03)
Gallbladder	4.40E-02 (1.01E-03)	1.63E-01 (4.04E-03)
LLI	1.80E-02 (6.56E-04)	6.66E-02 (2.43E-03)
Stomach	2.34E-02 (3.06E-04)	8.66E-02 (1.01E-03)
ULI	2.34E-02 (3.06E-04)	8.66E-02 (1.18E-03)
Heart	5.98E-02 (2.35E-03)	2.21E-01 (9.02E-03)
Kidneys	3.57E-02 (3.21E-03)	1.32E-01 (1.20E-02)
Liver	3.30E-01 (2.02E-02)	1.22E+00 (7.55E-02)
Lungs	1.46E-02 (2.65E-04)	5.40E-02 (1.00E-03)
Muscle	1.83E-02 (4.58E-04)	6.78E-02 (1.72E-03)
Ovaries	1.91E-02 (6.56E-04)	7.07E-02 (2.34E-03)
Pancreas	3.17E-02 (2.0E-04)	1.17E-01 (5.77E-04)
Skin	1.52E-02 (4.58E-04)	5.62E-02 (1.67E-03)
Spleen	2.07E-01 (1.11E-02)	7.66E-01 (4.03E-02)
Testes	1.56E-02 (6.56E-04)	5.77E-02 (2.34E-03)
Thymus	1.92E-02 (5.00E-04)	7.11E-02 (2.00E-03)
Thyroid	1.64E-02 (6.11E-04)	6.06E-02 (2.33E-03)
Urinary	1.78E-02 (6.66E-04)	6.60E-02 (2.48E-03)
Uterus	1.90E-02 (6.56E-04)	7.04E-02 (2.38E-03)
Effective Dose	3.42E-02 (6.51E-04)	1.27E-01 (2.52E-03)

Abbreviations: LLI, lower large intestine; ULI: upper large intestine.

targeting due to the EPR effect of the tumor. For all the other tumors, the tracer uptake increased or remained steady over time, which is characteristic of specific targeting. In this study, the passive targeting of GL-26 is quite prominent and, at its peak, the uptake is even higher than integrin $\alpha_v\beta_3$-positive tumors MDA-MB-435 and PC-3. PET imaging of other tumors (e.g., C6 rat glioma) that are human/mouse integrin $\alpha_v\beta_3$ negative revealed a similar tracer uptake profile as the GL-26 tumor (data not shown), although the time point of maximum tumor uptake varied between these tumors because of the difference in vascular density and leakiness. The tracer uptake, tracer clearance, and the pharmacokinetics of ^{64}Cu-DOTA-Abegrin^{TM} are quite different from our previously reported RGD peptide-based imaging (29, 31, 48). The passive targeting of this antibody may provide a more general use in cancer therapy as most tumors have leaky vasculature, which may result in more uptake of Abegrin^{TM}-based agents and greater efficacy.

We realize that the pharmacokinetics of ^{64}Cu-DOTA-Abegrin^{TM} in the present study may not be a true mimicry of the clinical situation because Abegrin does not bind mouse integrin $\alpha_v\beta_3$. This may also be partially responsible for the faster tracer clearance. For future studies, other rodent models, such as hamsters or primates (Abegrin^{TM} cross-reacts with hamster and certain primate integrin $\alpha_v\beta_3$), may be used to obtain dosimetry instead of mice and rats. Transgenic mouse models that express both human and mouse integrin $\alpha_v\beta_3$ may also be relevant. Due to both the heterogeneity of the tumor itself and the weaker tissue penetration of the mAb-based tracer because of its large molecular weight, the tracer uptake in the tumor is also somewhat heterogeneous. As can be seen from Fig. 1*A*, the tracer uptake of the U87MG tumor is higher in the periphery region of the tumor and significantly lower in the center of the tumor, although *ex vivo* examination revealed that the tumor center was not necrotic.

In summary, we describe here the *in vitro* and *in vivo* characterization of ^{64}Cu-labeled Abegrin^{TM}, a humanized mAb against human integrin $\alpha_v\beta_3$, in various tumor models. No significant difference in immunoreactivity was found among the five ^{64}Cu-DOTA-Abegrin^{TM} conjugates tested. MicroPET imaging of ^{64}Cu-DOTA-Abegrin (1,000:1) showed U87MG tumor uptake as high as 49.41 $\pm$ 4.54 %ID/g at 71-hour postinjection. The success of human integrin $\alpha_v\beta_3$-specific tumor imaging using ^{64}Cu-DOTA-Abegrin^{TM} may be translated into the clinic to evaluate the pharmacokinetics, tumor targeting efficacy, dose optimization, and dose interval of Abegrin and Abegrin-based cancer therapeutics. A certain level of nonspecific targeting due to the leaky vasculature of the tumors may also have potential applications in radioimmunotherapy in general.

Acknowledgments

Received 4/24/2006; revised 6/14/2006; accepted 8/1/2006.

Grant support: MedImmune, National Institute of Biomedical Imaging and Bioengineering grant R21 EB001785, National Cancer Institute (NCI) grant R21 CA102123, NCI In Vivo Cellular Molecular Imaging Center grant P50 CA114747, NCI Small Animal Imaging Resource Program grant R24 CA93862, NCI Centers of Cancer Nanotechnology Excellence U54 grant 1U54CA119367-01, Department of Defense (DOD) Breast Cancer Research Program IDEA Award W81XWH-04-1-0697, DOD Ovarian Cancer Research Program Award OC050120, DOD Prostate Cancer Research Program New Investigator Award DAMD1717-03-1-0143, and Education and Research Foundation of the Society of Nuclear Medicine Benedict Cassen Postdoctoral Fellowship (W. Cai).

The costs of publication of this article were defrayed in part by the payment of page charges. This article must therefore be hereby marked *advertisement* in accordance with 18 U.S.C. Section 1734 solely to indicate this fact.

We thank Ms. Pauline Chu and Dr. Xianzhong Zhang for their excellent technical support and the cyclotron teams of Washington University and University of Wisconsin for ^{64}Cu production.

References

1. Bergers G, Benjamin LE. Tumorigenesis and the angiogenic switch. Nat Rev Cancer 2003;3:401–10.
2. Nyberg P, Xie L, Kalluri R. Endogenous inhibitors of angiogenesis. Cancer Res 2005;65:3967–79.
3. Friedl P, Wolf K. Tumour-cell invasion and migration: diversity and escape mechanisms. Nat Rev Cancer 2003; 3:362–74.
4. Brooks PC, Clark RA, Cheresh DA. Requirement of vascular integrin $\alpha_v\beta_3$ for angiogenesis. Science 1994;264: 264:569–71.
5. Hood JD, Cheresh DA. Role of integrins in cell invasion and migration. Nat Rev Cancer 2002;2:91–100.
6. Xiong JP, Stehle T, Diefenbach B, et al. Crystal structure of the extracellular segment of integrin $\alpha_v\beta_3$. Science 2001;294:339–45.
7. Kumar CC. Integrin $\alpha_v\beta_3$ as a therapeutic target for blocking tumor-induced angiogenesis. Curr Drug Targets 2003;4:123–31.
8. Meerovitch K, Bergeron F, Leblond L, et al. A novel RGD antagonist that targets both $\alpha_v\beta_3$ and $\alpha_5\beta_1$ induces apoptosis of angiogenic endothelial cells on type I collagen. Vascul Pharmacol 2003;40:77–89.
9. Brooks PC, Stromblad S, Sanders LC, et al. Localization of matrix metalloproteinase MMP-2 to the surface of invasive cells by interaction with integrin $\alpha_v\beta_3$. Cell 1996;85:683–93.
10. Cai W, Chen X. Anti-angiogenic cancer therapy based on integrin $\alpha_v\beta_3$ antagonism. Anti-Cancer Agents Med Chem 2006;6:407–28.
11. Cheresh DA. Human endothelial cells synthesize and express an arg-gly-asp-directed adhesion receptor involved in attachment to fibrinogen and von Willebrand factor. Proc Natl Acad Sci U S A 1987; 84:6471–5.
12. Carter P. Improving the efficacy of antibody-based cancer therapies. Nat Rev Cancer 2001;1:118–29.
13. Wu H, Beuerlein G, Nie Y, et al. Stepwise *in vitro* affinity maturation of Vitaxin, an $\alpha_v\beta_3$-specific humanized mAb. Proc Natl Acad Sci U S A 1998;95:6037–42.
14. Patel SR, Jenkins J, Papadopolous N, et al. Pilot study of Vitaxin-an angiogenesis inhibitor-in patients with advanced leiomyosarcomas. Cancer 2001;92:1347–8.
15. Gutheil JC, Campbell TN, Pierce PR, et al. Targeted antiangiogenic therapy for cancer using Vitaxin: a humanized monoclonal antibody to the integrin $\alpha_v\beta_3$. Clin Cancer Res 2000;6:3056–61.
16. Posey JA, Khazaeli MB, DelGrosso A, et al. A pilot trial of Vitaxin, a humanized anti-vitronectin receptor (anti $\alpha_v\beta_3$) antibody in patients with metastatic cancer. Cancer Biother Radiopharm 2001;16:125–32.
17. McNeel DG, Eickhoff J, Lee FT, et al. Phase I trial of a monoclonal antibody specific for $\alpha_v\beta_3$ integrin (MEDI-522) in patients with advanced malignancies, including an assessment of effect on tumor perfusion. Clin Cancer Res 2005;11:7851–60.
18. Woessner R, Kiener P, Dormitzer M, Walsh W, Heinrichs J, (Medimmune, Inc., USA). The prevention or treatment of cancer using integrin $\alpha_v\beta_3$ antagonists, such as anti-integrin $\alpha_v\beta_3$ antibody Vitaxin, in combination with other agents. US patent 2003-US6684. 2003.
19. Chen X, Conti PS, Moats RA. *In vivo* near-infrared fluorescence imaging of integrin $\alpha_v\beta_3$ in brain tumor xenografts. Cancer Res 2004;64:8009–14.
20. Cai W, Shin DW, Chen K, et al. Peptide-labeled near-infrared quantum dots for imaging tumor vasculature in living subjects. Nano Lett 2006;6:669–76.
21. Sipkins DA, Cheresh DA, Kazemi MR, Nevin LM, Bednarski MD, Li KC. Detection of tumor angiogenesis *in vivo* by $\alpha_v\beta_3$-targeted magnetic resonance imaging. Nat Med 1998;4:623–6.
22. Winter PM, Caruthers SD, Kassner A, et al. Molecular imaging of angiogenesis in nascent Vx-2 rabbit tumors using a novel $\alpha_v\beta_3$-targeted nanoparticle and 1.5 tesla magnetic resonance imaging. Cancer Res 2003;63:5838–43.
23. Ellegala DB, Leong-Poi H, Carpenter JE, et al. Imaging tumor angiogenesis with contrast ultrasound and microbubbles targeted to $\alpha_v\beta_3$. Circulation 2003;108: 336–41.
24. Janssen ML, Oyen WJ, Dijkgraaf I, et al. Tumor targeting with radiolabeled $\alpha_v\beta_3$ integrin binding peptides in a nude mouse model. Cancer Res 2002;62: 6146–51.
25. Meoli DF, Sadeghi MM, Krassilnikova S, et al. Noninvasive imaging of myocardial angiogenesis following experimental myocardial infarction. J Clin Invest 2004;113:1684–91.
26. Chen X, Hou Y, Tohme M, et al. Pegylated Arg-Gly-Asp peptide: ^{64}Cu labeling and PET imaging of brain tumor $\alpha_v\beta_3$-integrin expression. J Nucl Med 2004;45: 1776–83.
27. Haubner R, Wester H-J, Weber WA, et al. Noninvasive imaging of $\alpha_v\beta_3$ integrin expression using ^{18}F-labeled RGD-containing glycopeptide and positron emission tomography. Cancer Res 2001;61:1781–5.
28. Chen X, Park R, Hou Y, et al. MicroPET imaging of brain tumor angiogenesis with ^{18}F-labeled PEGylated RGD peptide. Eur J Nucl Med Mol Imaging 2004;31: 1081–9.
29. Zhang X, Xiong Z, Wu X, et al. Quantitative PET imaging of tumor integrin $\alpha_v\beta_3$ expression with ^{18}F-FRGD2. J Nucl Med 2006;47:113–21.
30. Chen X, Park R, Shahinian AH, et al. ^{18}F-labeled RGD peptide: initial evaluation for imaging brain tumor angiogenesis. Nucl Med Biol 2004;31:179–89.
31. Wu Y, Zhang X, Xiong Z, et al. MicroPET imaging of

glioma α_v-integrin expression using ^{64}Cu-labeled tetrameric RGD peptide. J Nucl Med 2005;46:1707–18.
32. Chen X, Park R, Tohme M, Shahinian AH, Bading JR, Conti PS. MicroPET and autoradiographic imaging of breast cancer α_v-integrin expression using ^{18}F- and ^{64}Cu-labeled RGD peptide. Bioconjug Chem 2004;15:41–9.
33. Haubner R, Weber WA, Beer AJ, et al. Noninvasive visualization of the activated $\alpha_v\beta_3$ integrin in cancer patients by positron emission tomography and [^{18}F]galacto-RGD. PLoS Med 2005;2:e70.
34. Chen X, Sievers E, Hou Y, et al. Integrin $\alpha_v\beta_3$-targeted imaging of lung cancer. Neoplasia 2005;7:271–9.
35. Beer AJ, Haubner R, Goebel M, et al. Biodistribution and pharmacokinetics of the $\alpha_v\beta_3$-selective tracer ^{18}F-galacto-RGD in cancer patients. J Nucl Med 2005;46:1333–41.
36. Cai W, Zhang X, Wu Y, Chen X. A thiol-reactive ^{18}F-labeling agent N-[2-(4-^{18}F-fluorobenzamido)ethyl]-maleimide (^{18}F-FBEM) and the synthesis of RGD peptide-based tracer for PET imaging of $\alpha_v\beta_3$ integrin expression. J Nucl Med. 2006;47:1172–80.
37. Chen X, Tohme M, Park R, Hou Y, Bading JR, Conti PS. Micro-PET imaging of $\alpha_v\beta_3$-integrin expression with ^{18}F-labeled dimeric RGD peptide. Mol Imaging 2004;3:96–104.
38. Haubner R, Wester HJ, Reuning U, et al. Radiolabeled $\alpha_v\beta_3$ integrin antagonists: a new class of tracers for tumor targeting. J Nucl Med 1999;40:1061–71.
39. Meares CF, McCall MJ, Reardan DT, Goodwin DA, Diamanti CI, McTigue M. Conjugation of antibodies with bifunctional chelating agents: isothiocyanate and bromoacetamide reagents, methods of analysis, and subsequent addition of metal ions. Anal Biochem 1984;142:68–78.
40. Lindmo T, Boven E, Cuttitta F, Fedorko J, Bunn PA, Jr. Determination of the immunoreactive fraction of radiolabeled monoclonal antibodies by linear extrapolation to binding at infinite antigen excess. J Immunol Methods 1984;72:77–89.
41. Chen X, Plasencia C, Hou Y, Neamati N. Synthesis and biological evaluation of dimeric RGD peptide-paclitaxel conjugate as a model for integrin-targeted drug delivery. J Med Chem 2005;48:1098–106.
42. Sgouros G. Dosimetry of internal emitters. J Nucl Med 2005;46 Suppl 1:18–27S.
43. Cutler PD, Schwarz SW, Anderson CJ, et al. Dosimetry of copper-64-labeled monoclonal antibody 1A3 as determined by PET imaging of the torso. J Nucl Med 1995;36:2363–71.
44. Venditto VJ, Regino CA, Brechbiel MW. PAMAM dendrimer based macromolecules as improved contrast agents. Mol Pharm 2005;2:302–11.
45. Verel I, Visser GW, Boellaard R, et al. Quantitative ^{89}Zr immuno-PET for *in vivo* scouting of ^{90}Y-labeled monoclonal antibodies in xenograft-bearing nude mice. J Nucl Med 2003;44:1663–70.
46. Bello L, Francolini M, Marthyn P, et al. $\alpha_v\beta_3$ and $\alpha_v\beta_5$ integrin expression in glioma periphery. Neurosurgery 2001;49:380–9.
47. Max R, Gerritsen RR, Nooijen PT, et al. Immunohistochemical analysis of integrin $\alpha_v\beta_3$ expression on tumor-associated vessels of human carcinomas. Int J Cancer 1997;71:320–4.
48. Chen X, Park R, Shahinian AH, Bading JR, Conti PS. Pharmacokinetics and tumor retention of ^{125}I-labeled RGD peptide are improved by PEGylation. Nucl Med Biol 2004;31:11–9.